Journal of the European Ceramic Society **8** (1991) 81–93

Kinetics of Capillary Extraction of Organic Vehicle from Ceramic Bodies. Part I: Flow in Porous Media

Y. Bao & J. R. G. Evans

Department of Materials Technology, Brunel University, Uxbridge, Middlesex UB8 3PH, UK

(Received 14 January 1991; accepted 18 March 1991)

Abstract

Gas and water flow permeabilities of four powder beds with diverse characteristics were measured and compared with values predicted by a range of model equations. No single equation was found to fit all powders. This means that a general theory of capillary extraction of ceramic binders cannot rest on currently available permeability models. The kinetics of wax sorption from an unlimited supply was measured gravimetrically and was found to have parabolic dependence on time, as predicted by Darcy's Law. The sorption constant was deduced and, together with experimental values of permeability, used to calculate the average capillary pressures for the powder beds. These in turn were compared with theory. In Part II the results will be used to attempt to quantify the extraction of wax from ceramic bodies.

An vier Pulverschüttungen mit unterschiedlichen Eigenschaften wurden die Permeabilitäten für Gas und Wasser gemessen und mit theoretisch berechneten Werten mehrerer Modelle verglichen. Keine Einzige dieser Gleichungen konnte alle vier Pulver korrekt beschreiben. Dies bedeutet, daß eine allgemeingültige Theorie über das Entfernen der Bindephase aus keramischen Formkörpern mittels kapillarer Kräfte durch zur Zeit verfügbare Permeabilitätsmodelle nicht aufgestellt werden kann. Die Kinetik der Wachsaufnahme unter der Randbedingung einer unbegrenzten Wachsmenge wurde gravimetrisch gemessen und gehorcht, wie Darcy's Gleichung vorhersagt, einem parabolischen Zeitgesetz. Die Sorptionskonstante wurde abgeleitet und, zusammen mit den experimentell bestimmten Permeabilitäten, dazu verwendet, die durchschnittlichen Kapillardrücke der Pulverschüttungen zu berechnen. Diese wurden mit den theoretischen Werten verglichen. In Teil 2 wird versucht anhand dieser Ergebnisse den Entzug des Wachses aus keramischen Formkörpern quantitativ zu erfassen.

Les valeurs de perméabilité d'écoulement de gaz et d'eau de quatre lits de poudres présentant diverses caractéristiques ont été mesurées et comparées avec les valeurs prévues par une série d'équation types. On n'a pas trouvé d'équation unique qui corresponde à l'ensemble des poudres étudiées. Cela signifie qu'une théorie générale de l'extraction capillaire des liants céramiques ne peut pas reposer sur les modèles de perméabilité dont on dispose couramment. Les cinétiques de sorption de la cire en alimentation continue ont été mesurées gravimétriquement en dépendent du temps de manière parabolique comme le prévoit la loi de Darcy. On en a déduit la constante de sorption et, en utilisant conjointement les valeurs experimentales de perméabilité, on a pu calculer les pressions capillaires moyennes pour les lits de poudres. Les résultats ont ensuite été comparés avec la théorie et seront utilisés dans la partie 2 pour tenter de quantifier l'extraction de la cire de pièces céramiques.

Notation

a, b, c	Empirical constants
A	Cross-sectional area of flow path (m^2)
A_v	Constant in the Mark–Houwink equation
C	Kozeny constant
D	Average particle size (m)
D_c	Equivalent capillary diameter (m)
D_e	Hydraulic pore diameter (m)
E	Fractional porosity of any porous body
E_d	Fractional porosity of the ceramic body
E_{eff}	Effective porosity of the powder bed

E_p Fractional porosity of the powder bed
f Ratio of the length of liquid column in the powder bed to the total length of the liquid column
H Length of liquid column inside the ceramic body (m)
ΔH Activation energy (kJ mol^{-1})
$J(s)$ Leverett function
K Sorption constant (m s$^{-1/2}$)
K_d Average permeability of the ceramic body (m^2)
K_{eff} Effective permeability for the coupled system (m^2)
K_p Average permeability of the powder bed (m^2)
L Total length of the liquid column (m)
L_p Thickness of the powder bed in permeability tests (m)
M_w Molecular weight of polymer (g mol^{-1})
ΔP Pressure difference causing flow in a porous body (Pa)
ΔP_c Average capillary pressure difference between powder bed and ceramic body (Pa)
P_c Average capillary pressure (Pa)
P_0 Inlet absolute pressure of the gas flow apparatus (Pa)
P_1 Outlet absolute pressure of the gas flow apparatus (Pa)
Q_g Volume flow rate of gas (m^3 s^{-1})
R Gas constant (J mol^{-1} K^{-1})
$\bar{R}$ Mean particle radius (m)
Re Reynolds number
s Saturation (filled pore volume divided by available pore volume)
s_d Saturation of ceramic body
s_p Saturation of powder bed
S_0 Specific surface area per unit solid volume (m^{-1})
S_v Specific surface area of the porous medium (m^{-1})
t Sorption time (s)
t_0 Duration of the transient stage (s)
t_{50} Time required for the exodus of 50% of the available wax (s)
T Temperature of the fluid (K)
T_c Critical temperature of the fluid (K)
$v(x)$ The volume of liquid uptake by a powder bed of unit area (m)
$V(x)$ The volume of liquid uptake by the powder bed (m^3)
V_c The volume fraction of ceramic powder in the powder bed
V_i The initial volume of wax in the ceramic body (m^3)
V_w The volume fraction of organic vehicle in the powder bed
V_0 The volume of wax removed in the transient stage (m^3)
x The coordinate along the flow direction in the powder bed (m)
X_w The weight fraction of organic vehicle in the powder bed
Z Average compressibility factor of fluid evaluated at $P/2$
Z_{eff} Effective compressibility factor of fluid

α Empirical constant
γ Surface energy of liquid (J m^{-2})
γ_0 Surface energy of liquid at zero temperature (J m^{-2})
η Viscosity of the fluid (Pa s)
θ Contact angle of the liquid on the solid (°)
ρ_g Density of a gas (kg m^{-3})
ρ_p Density of the powder bed (kg m^{-3})
ρ_w Density of the organic vehicle (kg m^{-3})

1 Introduction

Injection moulding and related manufacturing processes for ceramics require that the entire pore space be filled with an organic vehicle.[1,2] Once the shaping operation is complete, the vehicle must be removed prior to firing without damaging the assembly of particles. Controlled pyrolysis is the favoured way of achieving this goal[3] but for large sections this can result in defects caused by the boiling of low molecular weight products of decomposition in solution in molten polymers or waxes. Since large volumes of gaseous product are associated with pyrolysis,[4] methods which remove the organic phase in the liquid state are an advantage. Thus Curry[5] and Wiech[6] describe the extraction of low viscosity liquids by placing the ceramic body in contact with a loose powder or a porous tile. A similar procedure is used in the removal of wax from relatively coarse metal powder mouldings.[7] German[8] has quantified the time required for binder removal by applying a model for the permeability of powder beds in terms of average particle size and porosity. When this procedure was applied to fine ceramic powders, the calculated times did not agree well with experiment and the assumption that the ceramic body controlled the rate of flow was found to be inappropriate for powder beds composed of fine powders.[4] Furthermore, it was clear that only a fraction of the available pore space in the powder was used. Rather than flow as a

column out of the ceramic body, the wax was uniformly distributed throughout the body, but a decrease in saturation accompanied extraction.

In the light of these observations, the present work seeks to quantify the process of capillary extraction. In the first place, the several expressions for permeability and average capillary pressure of porous media in terms of particle characteristics are reviewed. The expressions for permeability are compared with gas flow permeabilities. Gas flow permeabilities are in turn compared with permeabilities deduced from wax sorption experiments from an unlimited supply. In the second stage of the work, the unlimited supply of wax is replaced with a ceramic body so that the effect of the opposing capillary pressure and additional resistance to flow can be deduced.

2 Equations for Flow in Porous Media

The kinetics of flow in the powder bed can be studied by suspending a packed column in contact with the surface of a molten liquid bath, as in the method of Beltran *et al.*[9] The liquid column is assumed to rise a distance x through numerous capillary channels such that for the duration of the experiment the pressure of the column associated with gravity is very much less than the capillary pressure. According to Darcy's law, the volumetric rate of liquid uptake by the powder is

$$\frac{dV(x)}{dt} = -\frac{K_p \Delta P A}{\eta x} \tag{1}$$

where η is the dynamic viscosity of the liquid at the temperature under consideration, K_p is the average permeability of the powder bed, and ΔP is the pressure difference between x and the liquid surface, and is a negative term if the pressure gradient is taken in the direction of flow.

If E is the fractional porosity of the powder bed and s is the fractional saturation of the available pore space then

$$V(x) = xEsA \tag{2}$$

and the rate of uptake becomes

$$\frac{dV(x)}{dt} = \frac{K_p \Delta P E s A^2}{\eta V(x)} \tag{3}$$

Integrating eqn (3) with lower limits $t = 0$, $V(x) = 0$ and solving for $V(x)$ gives

$$V^2(x) = 2K_p \Delta P E s A^2 t/\eta \tag{4}$$

or

$$v^2(x) = \left[\frac{V(x)}{A}\right]^2 = \frac{2K_p \Delta P E s t}{\eta} \tag{5}$$

where $v(x)$ is the volume absorbed per unit area at time t. The rate of uptake is thus dependent on the pressure difference ΔP, the permeability of the powder bed K_p and the viscosity of the liquid η.

The pressure term in capillarial porous media arises from the pressure defect associated with the curved liquid–vapour menisci in the capillary channels, but the average capillary pressure is a function of saturation of the porous medium.[10] Furthermore, it can be argued that only a fraction of the average capillary pressure induces flow in the x direction, and Carman[11] suggests that capillaries are randomly oriented with a mean angle of 45° to the direction of flow. If this is the case then

$$\Delta P = \frac{P_c}{\sqrt{2}} \tag{6}$$

where P_c is the average capillary pressure and eqn (5) becomes

$$v(x)^2 = \frac{\sqrt{2} K_p P_c E s t}{\eta} \tag{7}$$

or

$$v(x) = K t^{1/2} \tag{8}$$

where

$$K = \left(\frac{\sqrt{2} K_p P_c E s}{\eta}\right)^{1/2} \tag{9}$$

K is a constant for a given isothermal sorption experiment, hereinafter called the sorption constant, with units $m\,s^{-1/2}$.

3 Average Capillary Pressure

In order to quantify the capillary extraction of organic vehicle from ceramic bodies in such a way that meaningful predictions can be obtained from available powder and fluid properties, values of P_c and K_p are sought.

It is well known that for a circular capillary the capillary pressure can be expressed as

$$P_c = 4\gamma \cos\theta / D_c \tag{10}$$

where γ is the surface tension of the gas–liquid interface, θ is the contact angle of the liquid on the solid and D_c is the diameter of the capillary.

As the pore structure of the powder does not consist of circular capillaries having the same capillary diameter, eqn (10) cannot be applied

directly to a porous medium. Several modifications to eqn (10) have been devised, most of which assume a zero contact angle.

The Carman equation[11] obtained from a model for straight capillaries yields

$$P_c = \frac{\gamma S_v}{E} \tag{11}$$

where S_v is the pore specific surface area of the porous medium, and

$$S_v = (1 - E)S_0 \tag{12}$$

where S_0 is the specific surface area per unit solid volume.

Leverett[10,12] derived a dimensionless expression to describe the dependence of P_c on saturation, which is extremely important where the extraction of fluids from ceramic bodies is concerned, because of the change in saturation of the body with time:[4]

$$J(s) = \frac{P_c}{\gamma}\left(\frac{K_p}{E}\right)^{1/2} \tag{13}$$

where $J(s)$ is termed the Leverett function.

Oyama & Yamaguchi[13] considered the packing of regular spheres and proposed

$$P_c = \frac{9{\cdot}8\gamma \cos\theta}{D} \tag{14}$$

where D is the mean particle diameter. They dealt with porosities in the region of 48% corresponding to simple cubic packing, which is somewhat lower than the porosity of unconsolidated powder beds. Their particles were glass beads in the diameter range 800–4000 μm.

Luikov[14] derived from equivalent sphere-packing theory three expressions for critical capillary pressure corresponding to different states of saturation. The funicular regime describes intermediate saturation in which porosity develops in the continuous liquid phase:

$$P_c = 4{\cdot}1\gamma/\bar{R} \quad \text{(for imbibation at the start of the funicular regime)} \tag{15a}$$

$$P_c = 6{\cdot}9\gamma/\bar{R} \quad \text{(for imbibation at the start of the capillary state)} \tag{15b}$$

$$P_c = 12{\cdot}9\gamma/\bar{R} \quad \text{(for drainage from the capillary state to the funicular regime)} \tag{15c}$$

where $\bar{R}$ is the mean particle radius.

Expressions (10)–(15) arise from different geometrical models for the pore structure in the porous medium. In order to compare them a monodisperse powder with 1 μm diameter spheres which is packed to give a fractional porosity of 0·7 is considered.

Table 1. Comparison of equations for average capillary pressure and permeability for a 1 μm diameter monodisperse powder with a fractional porosity of 0·7

Equation number	*Average capillary pressure* ($\times 10^6\ Nm^{-2}$)	*Permeability* ($\times 10^{-14}\ m^2$)
(11)	2·57	
(14)	10	
(15)	2·58 1·38 0·82	
(16)		5·3 5·9 6·3 7·1
(17)		2·1
(20)		3·0
(21)		2·5

Table 1 compares the values for capillary pressure from these diverse equations. These vary by a factor of 12.

4 Average Permeability

Like average capillary pressure models, various permeability models are based on their own assumptions for the structure of porous media. The following are often cited:

Kozeny's equation[15] for permeability takes the form

$$K_p = CE^3/S_v^2 \tag{16}$$

where C is called the 'Kozeny constant' and depends on the shape of the capillary cross-section. For a circle $C = 0{\cdot}5$, for a square $C = 0{\cdot}5619$, for an equilateral triangle $C = 0{\cdot}5974$, and for a strip $C = 2/3$.

The Kozeny equation was modified by Carman[16] to give

$$K_p = E^3/5S_0^2(1 - E)^2 \tag{17}$$

Ergun & Orning[17] incorporate a factor which modifies the pressure drop in the porous body due to viscous flow by a constant α:

$$K_p = E^3/2\alpha S_0^2(1 - E)^2 \tag{18}$$

where $1{\cdot}7 \leq \alpha \leq 3{\cdot}0$.

Meyer & Smith[18] suggested that for the steady flow of a compressible fluid

$$K_p = E^{4{\cdot}1}Z/2{\cdot}5S_v^2 Z_{eff} \tag{19}$$

where Z is the average compressibility factor of fluid evaluated at $\Delta P/2$ and Z_{eff} is the effective compressibility factor of fluid.

By taking $Z = Z_{eff}$ for incompressible fluids and $D = 6(1-E)/S_v$, German[8] has simplified eqn (19) to the form

$$K_p = E^4 D^2/90(1-E)^2 \quad (20)$$

Smith & Martin offered an empirical correlation:[19]

$$K_p = 190(E^2/S_v)^{2\cdot42} \quad (21)$$

Unfortunately, the majority of porous materials have extremely complex pore structures which are difficult to represent by a general geometrical model. Table 1 compares these equations for the case of a monodisperse 1 μm diameter spherical powder packed to a relative density of 0·3. Surprisingly, the estimates vary by a factor of only 3·4 for these conditions.

If a general equation is used to represent the above equations, it can be written as

$$K_p = aE^b S_v^c \quad (22)$$

where a, b and c are empirical parameters obtained by researchers through their own experimental models. In the present work, by using the permeability apparatus of Lea & Nurse,[20] gas flow measurements were made and the empirical parameters a, b and c in eqn (22) were obtained by least-squares regression from the experimental results. The applicability of eqns (16)–(21) was also tested by comparison with gas and water flow permeabilities.

5 Experimental Details

5.1 Materials

Details of the diverse alumina powders used are given in Table 2 and Fig. 1 presents scanning electron micrographs of these powders. The particle size distributions are given in Fig. 2. Powder LG20 was separated by sieving to give two grades labelled LA150 (150–90 μm) and LA75 (75–38 μm). These have a mean particle size of 120 and 60 μm, respectively, and volume-specific surface areas of

Table 2. Powder specifications

Powder grade[a]	*Purity (wt% Al_2O_3)*	*Mean size (μm)*	*Density ($kg\,m^{-3}$)*	*SSA*[c] *($m^2\,g^{-1}$)*	*Main crystalline phase*
RA6	99·4	0·9	3970	5	α-Al_2O_3
LG20	98·3	70[b]	3900	—	α-Al_2O_3
MA2LS	99·7	7·5	3970	0·3	α-Al_2O_3

[a] Source: Alcan Chemicals Ltd, UK.
[b] By SEM count.
[c] Specific surface area.

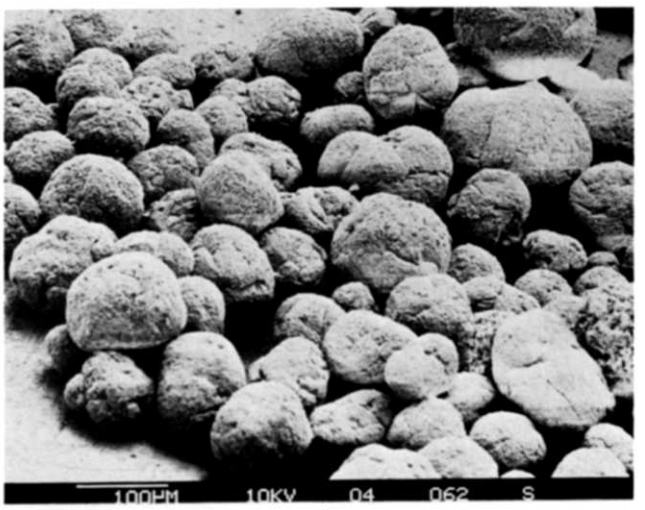

(a)

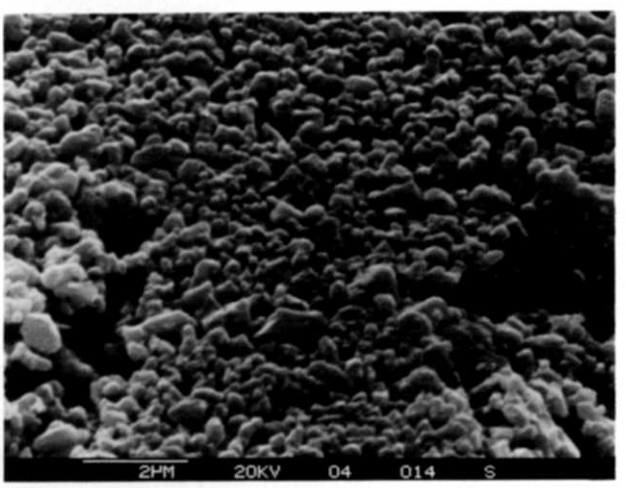

(b)

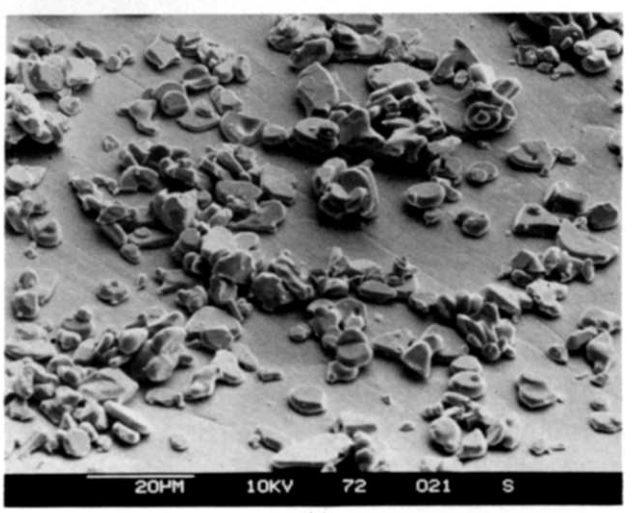

(c)

Fig. 1. Scanning electron micrographs of powders: (a) LG20; (b) RA6; (c) MA2LS.

$5{\cdot}2 \times 10^4\,m^{-1}$ and $1{\cdot}0 \times 10^5\,m^{-1}$, respectively, calculated from the mean particle size for narrow distributions. The organic vehicle was a paraffin wax, the details of which are given in Table 3.

The alumina powder density was found by density bottle determination, and the density of the powder

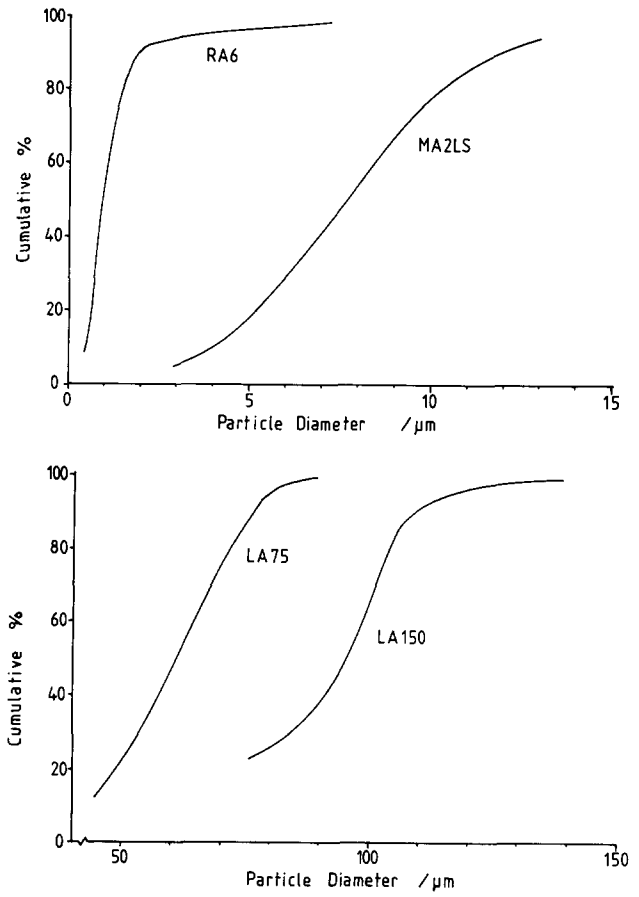

Fig. 2. Particle size distributions of the alumina powders.

bed was determined from bulk dimensions and weight measurement following the standard ISO 903 test method. Since the density of the bed (untapped) is sensitive to external vibration and applied pressure, the average of five measurements was taken. The maximum error was ±1·8%.

5.2 Gas flow apparatus and measurement

Gas flow testing was performed with nitrogen at room temperature, with an apparatus similar to that used by Lea & Nurse.[20] The powder was first compressed to a known porosity in a cell with a plunger. The bulk dimensions of powder beds were 25·4 mm in diameter and approximately 10 mm in thickness. The nitrogen volume flow was recorded on a flow meter (Model R53/R, Glass Precision Engineering, Herts, UK) and the pressure drop was measured on a mercury manometer. The volume flow of nitrogen through each powder bed was measured as a function of pressure drop. Porosity of the powder beds was varied by applying different pressures to the plunger during compaction.

Before measurement a series of empty flow tests for the apparatus were carried out at different pressures so as to establish the resistance of a supporting filter paper and metal gauze to the flow of gas. Estimated measurement accuracies for pressure and volume flow rate data were ±133·32 Pa, $\pm 1{\cdot}22 \times 10^{-5}$ m^3 s^{-1}, respectively.

Water flow permeability was measured by the method described by Scheidegger (Ref. 21, p. 92) using distilled water at 20°C, for which the viscosity was taken as 1·008 mPa s. The results are the average of permeability measured at three pressure differences.

Table 3. Binder characteristics of the paraffin wax[a]

Identification	Grade 130/135
Source	Shell Chemicals UK Ltd
Melting point (°C)	56 (ASTM)
Density at 20°C (kg m^{-3})	916
Density at 80°C (kg m^{-3})	766

[a] Data from manufacturer.

5.3 Liquid sorption experiments

Figure 3 shows the liquid sorption apparatus and the powder bed holder, which allows sections of the bed to be removed and ashed separately. The weight of fluid absorbed by powder beds was measured as a function of sorption time. The weight was determined from ashing the powder bed to 600°C in air.

The powder bed was first compressed to a known porosity in the powder bed holder. The powder bed was placed in an oven previously set to a constant temperature of 80°C and three hours were allowed for attainment of thermal equilibrium before sorption testing was started. The sorption time was recorded from the moment at which the powder bed touched the liquid surface. It was immersed to a depth of about 3 mm. The liquid container was large enough for the small variation of liquid level during sorption testing to be ignored. The plunger and thread were sufficiently loose to prevent a back pressure developing.

Each measurement was repeated three times to ensure reproducibility and the average of three results was obtained. Time, temperature and weight were estimated to an accuracy of ±5 s, ±1°C and ±0·01 g, respectively. Volume flow rates were calculated using the wax density measured at the test temperature.

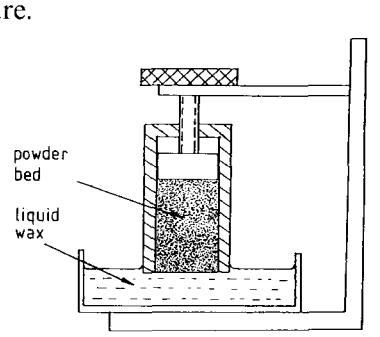

Fig. 3. Apparatus used for liquid sorption tests.

Table 4a. Gas flow experimental data and permeability (K_p)

Powder bed	*Porosity (%)*	S_v ($\times 10^6 m^{-1}$)	*Experimental* K_p ($\times 10^{-12} m^2$)	*Reynolds number*	*Calculated* K_p ($\times 10^{-12} m^2$)		
					Eqn (17)	*Eqn (20)*	*Eqn (21)*
LA75	68·5	0·033	1·7	0·37	59	89	350
	69·0	0·033	1·8	0·38	62	94	380
	70·0	0·032	2·4	0·40	69	107	440
	70·4	0·031	2·6	0·41	71	112	460
	72·0	0·030	4·9	0·44	86	137	592
	74·0	0·027	5·5	0·49	108	177	810
RA6	59·6	8·03	0·30	0·001 0	$6{\cdot}6 \times 10^{-4}$	$7{\cdot}0 \times 10^{-3}$	$3{\cdot}0 \times 10^{-4}$
	61·6	7·63	0·40	0·001 5	$8{\cdot}0 \times 10^{-4}$	$8{\cdot}9 \times 10^{-3}$	$4{\cdot}0 \times 10^{-4}$
	67·0	6·55	0·70	0·001 8	$1{\cdot}4 \times 10^{-3}$	$1{\cdot}7 \times 10^{-2}$	$8{\cdot}8 \times 10^{-4}$
	67·4	6·46	0·83	0·001 9	$1{\cdot}5 \times 10^{-3}$	$1{\cdot}8 \times 10^{-2}$	$9{\cdot}3 \times 10^{-4}$
	70·4	5·88	2·9	0·002 2	$2{\cdot}0 \times 10^{-3}$	$2{\cdot}5 \times 10^{-2}$	$1{\cdot}4 \times 10^{-3}$
	72·2	5·52	4·0	0·002 4	$2{\cdot}5 \times 10^{-3}$	$3{\cdot}2 \times 10^{-2}$	$1{\cdot}9 \times 10^{-3}$
	74·1	5·14	4·6	0·002 6	$3{\cdot}1 \times 10^{-3}$	$4{\cdot}0 \times 10^{-2}$	$2{\cdot}6 \times 10^{-3}$
MA2LS	58·1	0·499	0·27	0·019	0·16	0·41	0·22
	60·3	0·473	0·33	0·023	0·20	0·52	0·30
	61·0	0·465	0·36	0·022	0·21	0·57	0·33
	61·5	0·459	0·42	0·024	0·22	0·60	0·36
	66·2	0·403	0·48	0·030	0·36	1·05	0·71
	66·8	0·396	0·50	0·030	0·38	1·13	0·76
	74·0	0·310	1·20	0·043	0·85	2·8	2·3
LA150	69·2	0·014	6·3	0·86	319	387	2 800
	71·3	0·013	6·9	0·96	401	502	3 800
	74·3	0·012	8·2	2·6	566	738	6 100

Table 4b. Water flow experimental data and permeability (K_p)

Powder bed	*Porosity (%)*	S_v ($\times 10^6 m^{-1}$)	*Experimental* K_p ($\times 10^{-12} m^2$)	*Maximum Reynolds number*
LA75	71·3	0·03	2·1	0·04
RA6	71·3	5·7	0·65	$7{\cdot}65 \times 10^{-5}$
MA2LS	60·7	0·47	0·079	$1{\cdot}13 \times 10^{-4}$
LA150	70·8	0·014	5·8	0·012

6 Results and Discussion

6.1 Permeability of powder beds

The diverse powders selected cover a range of particle characteristics, notably particle size and shape (Figs 1 and 2), which are likely to influence capillary flow. RA6 is a fine submicron powder which is weakly agglomerated. LA75 is a coarse equiaxed powder while MA2LS is an intermediate size powder which has a rather plate-like particle shape.

When gas flows through a porous medium under certain conditions, discussed below, the relationship between the flow rate and the pressure can be described by Darcy's law directly.[22] Lindquist,[21] by a careful investigation of experimental results, came to the conclusion that Darcy's law is valid only for $Re < 4$.

In order to check if the gas flow measurement is in the region where Darcy's law is valid, the Reynolds number for each powder bed under the gas flow condition was first calculated using the flow equation:[22]

$$Re = Q_g \rho_g D_e / \eta A \tag{23}$$

where D_e is the hydraulic diameter of the powder bed[23] and is given by

$$D_e = 4E/(1 - E)S_0 \tag{24}$$

where Q_g is the volume flow rate of the gas, ρ_g is the density of the gas (in this case 1·25 kg m^{-3}), and S_0 is the volume-specific surface area of the powder.

The calculated results are listed in Table 4a. It can be seen that the Reynolds numbers of all powder beds under these experimental conditions are much less than 4. Thus Darcy's law is valid for these measurements.

The permeabilities of the powder beds were calculated from the measured flow rate, Q_g, and pressure, P, data according to Darcy's law for gas permeability:

$$Q_g = \frac{K_p A}{\eta L_p} \frac{P_1^2 - P_0^2}{2P_0} \tag{25}$$

where L_p is the thickness of the powder bed (in this

case 0·9–1·1 × 10^{-2} m), A is the cross-sectional area of the powder bed ($A = 5{\cdot}06 \times 10^{-4}$ m^2), η is the viscosity of nitrogen at the testing temperature ($\eta = 1{\cdot}74 \times 10^{-5}$ Pa s[24]), and subscripts 0 and 1 refer to inlet and outlet absolute pressures, respectively.

The experimental results are listed in Table 4a. For comparison, the permeabilities calculated using eqns (17), (20) and (21) are also given. As particle size changes, these equations present a much greater variation in K_p than that expected from Table 1; eqn (21) is especially sensitive to particle size.

Gas permeability results should correspond to liquid permeability results obtained in an apparatus with a fixed pressure difference (Ref. 21, p. 75), provided the restriction on the Reynolds number is observed and in the absence of reduction in pore size caused by adsorption. In order to confirm this, water permeability measurements were made on the same powders in the same porosity region (Table 4b). Leverett[10] also found slight discrepancies between gas flow and water flow permeabilities of packed columns.

Comparison of experimental and calculated permeabilities exposes a major difficulty in quantifying the capillary flow process. For the coarse LA75 and LA150 powders the calculated permeabilities are considerably higher than the experimental results. This is despite the fact that these powders are reasonably equiaxed (Fig. 1) and have a ratio of maximum to minimum particle size of less than 2. For such particle size distribution the calculated permeabilities should correspond reasonably well to predictions (Ref. 11, p. 35).

The problem is reversed in the case of the RA6 powder. Here the experimental results are larger than the calculated results by several orders of magnitude. This is easier to understand. The powder is loosely agglomerated so that permeability calculated on the basis of packing of individual particles neglects the larger interagglomerate pores. These large capillaries give a disproportionately high rate of flow which swamps the effect of the interparticle pores. The mean particle radius then has little relevance to the estimation of gas flow permeability. However, as will be discussed, it is the smaller pores which take part in the capillary extraction of wax.

Using the data in Table 4a, the permeabilities were fitted by a least-squares method to the porosity and the internal surface area of the powder beds. The experimental permeabilities of the powder beds can then be expressed as follows:

$$K_p = 0{\cdot}99E^{10{\cdot}3}S_v^{-1{\cdot}49} \quad \text{for RA6 powder bed} \quad (26)$$

$$K_p = 1{\cdot}0E^{10{\cdot}5}S_v^{-2{\cdot}22} \quad \text{for LA75 powder bed} \quad (27)$$

$$K_p = 0{\cdot}99E^{1{\cdot}39}S_v^{-2{\cdot}15} \quad \text{for MA2LS powder bed} \quad (28)$$

The multiple correlation coefficients are 0·94, 0·95 and 0·94, respectively. Insufficient data are available to obtain a correlation for the LA150 powder because it was not possible to obtain different packing efficiencies by pressing in the sorption cylinder.

Equations (26)–(28) show that, for a given powder bed, permeability is strongly dependent on the packing density of the bed, while in the case of similar porosity the permeability decreases with the increase of specific surface area of the powder. In each case the coefficient a in eqn (22) is close to unity.

The serious issue thrown up by Table 4a is that there is no single expression for permeability which accurately estimates the measured gas flow permeability of a diverse range of ceramic powders. The errors themselves are not systematic and clearly depend on particle characteristics which are not incorporated in existing models.

6.2 Sorption experiments from an unlimited supply

The purpose of the sorption tests was to verify the form of the flow eqns (8) and (9), and to obtain the sorption constants. All the experiments were carried out at 80°C. The thermogravimetric trace for paraffin wax shows[4] that in this temperature region the weight loss of paraffin wax caused by evaporation is negligible.

The sorption curves are represented graphically in the form of $v(x)$ versus $t^{1/2}$ according to eqn (8), and a straight line with a slope K is observed for each powder (Fig. 4) corresponding to the sorption constant. The K values of the powder beds were

Table 5. Saturation, effective porosity and sorption constant under conditions of unlimited liquid supply

Powder bed	*Bulk porosity* (%)	*Binder content* (*wt*%)	*Effective porosity* (%)	*Saturation* (*s*)	*K* ($m\,s^{-1/2}$)	*Correlation coefficient*
LA75	71·0	32·5	71·0	1·00	$1{\cdot}11 \times 10^{-3}$	0·995
LA150	71·0	32·0	69·4	0·97	$9{\cdot}03 \times 10^{-4}$	0·997
RA6	70·4	28·6	61·7	0·88	$6{\cdot}96 \times 10^{-4}$	0·999
MA2LS	68·8	22·0	45·7	0·66	$3{\cdot}81 \times 10^{-4}$	0·987

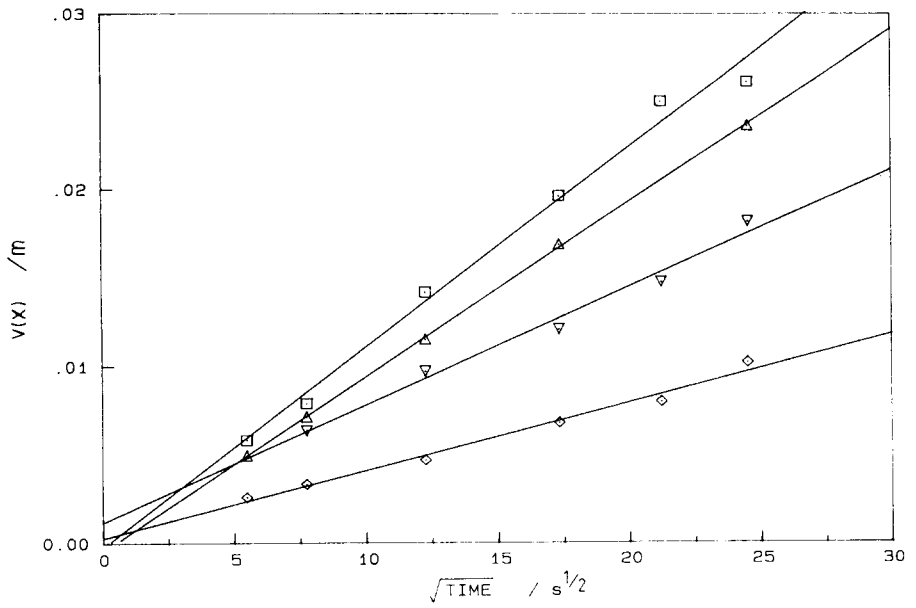

Fig. 4. Flow curves for calculation of sorption constant. Powder beds: ⊡, LA75; △, LA150; ▽, RA6; ◇, MA2LS.

determined by linear regression from the experimental results and are listed in Table 5 along with the correlation coefficients. From Fig. 4 and Table 5 it can be seen that there is a notable difference in sorption constant between different powder beds for a given binder at a fixed temperature, confirming the strong dependence on powder characteristics.

Both saturation and porosity enter the flow equation (eqn (9)). By definition

$$s = \frac{V_w}{1 - V_c} \tag{29}$$

where V_w is the volume fraction of organic vehicle in the powder bed based on the volume of the bed and V_c is the volume fraction of ceramic powder in the powder bed.

The relation between the volume fraction and the weight fraction of organic vehicle in a powder bed is given by

$$V_w = \frac{X_w}{1 - X_w} \frac{\rho_p}{\rho_w} \tag{30}$$

where X_w is the weight fraction of organic vehicle and ρ_p and ρ_w are the apparent density of the powder bed and the density of the organic vehicle, respectively.

Therefore, by measuring the wax content in the powder bed gravimetrically by ashing, the saturation of the powder bed can be obtained. The distribution of the liquid binder in the powder bed along the flow direction is shown in Fig. 5 for each powder studied. It can be seen that the liquid moved as a column so that saturation did not vary with position for the duration of the experiments, even in the case of incomplete saturation. The exact shape of the concentration profile at the head of the column cannot be deduced from the experiments because of the difficulty of obtaining a clean cut from the apparatus in Fig. 3 and the size of cuts taken, which limits resolution. The saturation and the volume fraction (V_w) of the binder based on the total volume are listed in Table 5. It can be seen that the saturations of RA6 and MA2LS powder bed are less than unity. The MA2LS powder bed, which has plate-like particles (see Fig. 2), has the lowest saturation. This partly explains the low sorption constant for these powders.

The low saturations of RA6 and MA2LS may be the result of local fracture of the bed caused by slight movement of the particles under the influence of capillary pressure, which could cause local fissures to form which do not fill, and even isolation of parts of the bed. This may be particularly prevalent in the MA2LS, which contains rather plate-like particles (Fig. 1(c)) capable of rearrangement to denser assemblies. It may also be associated with a wide distribution of effective pore sizes caused, in the case of RA6, by agglomeration.

That the saturations are less than unity means that not all pores in the powder bed are available to extract the liquid, even under conditions of unlimited wax supply, an observation also made by Leverett.[10] Thus the total porosity of a powder bed does not necessarily reflect its capacity to extract the liquid, nor by implication does it lead directly to the calculated permeability or average capillary pressure. Thus an effective porosity, E_{eff}, can be defined

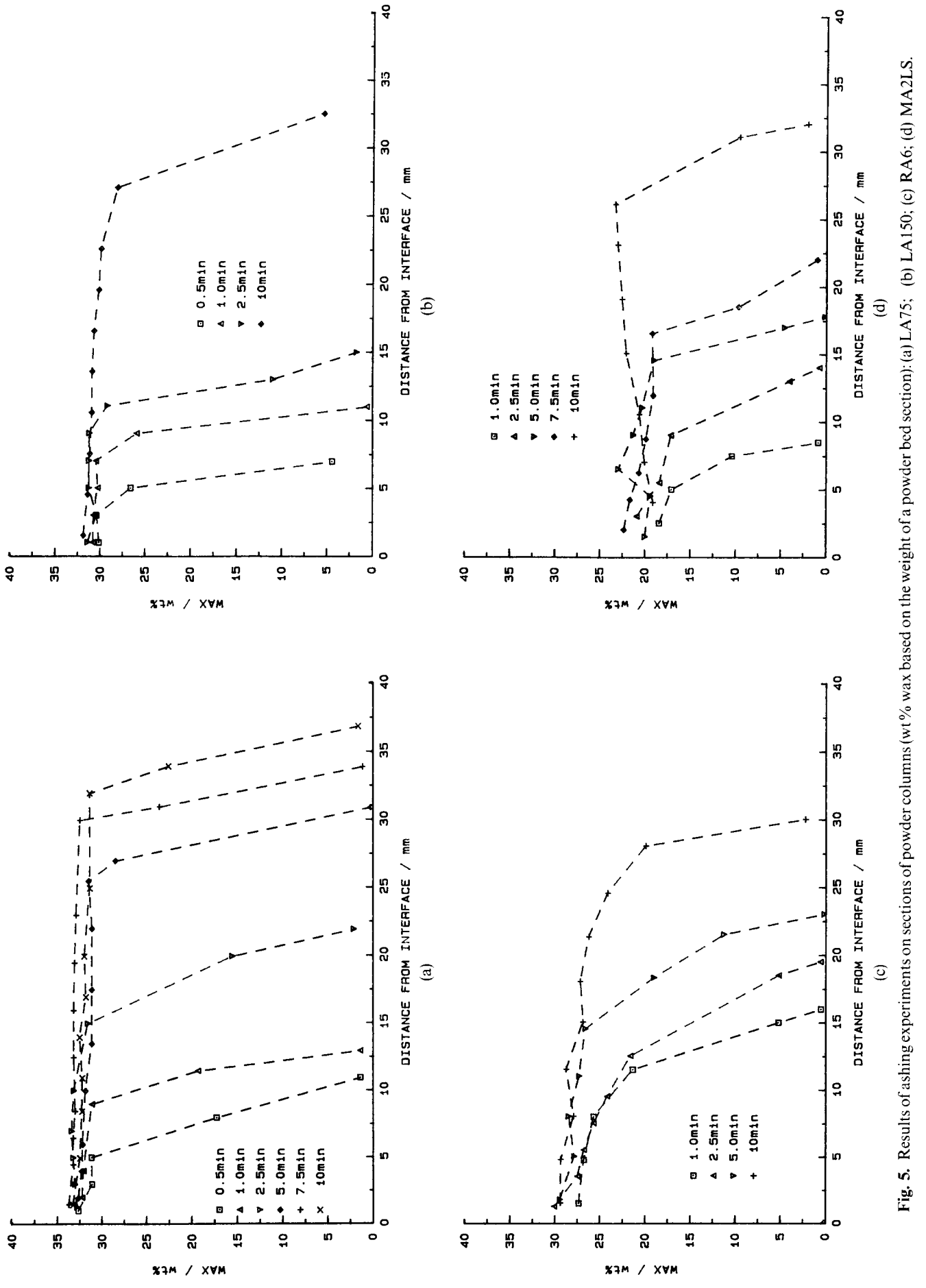

Fig. 5. Results of ashing experiments on sections of powder columns (wt % wax based on the weight of a powder bed section): (a) LA75; (b) LA150; (c) RA6; (d) MA2LS.

which is also equal to the volume fraction of organic vehicle in the powder bed:

$$E_{\text{eff}} = \frac{X_w}{1 - X_w} \frac{\rho_p}{\rho_w} = sE \tag{31}$$

6.3 Estimation of capillary pressures

Thus far the terms in eqn (9) have been obtained by experiment, and the difficulties of estimating K_p from powder properties have been highlighted. The problem that remains is the acquisition of P_c, the average capillary pressure of the powder bed, a quantity which is difficult to obtain experimentally.

Using the experimentally acquired data, P_c can be obtained by rearranging eqn (9) to give

$$P_c = \frac{K^2 \eta}{\sqrt{2} K_p E s} \tag{32}$$

Table 6 compares the value of P_c deduced in this way with values predicted by eqns (11), (13), (14), (15a) and (15b). For eqn (32) the value of K_p was calculated from eqns (26)–(28) using effective porosity. The validity of this approach is discussed more fully in Part II,[25] wherein effective porosities are much lower. The surface energy of the wax was taken as 29 mJ m^{-2},[26] and the viscosity at 80°C was 3·78 mPa s.[25]

In eqn (11) the ratio of the pore volume to the internal surface area of the powder bed is used to represent the hydraulic radius of the bed. This procedure gives a good fit for the two coarse powders, LA75 and LA150, but offers a rather large positive deviation for the RA6 and MA2LS powder beds. This means that eqn (11) cannot reflect the effect of non-uniform packing, such as that associated with agglomeration or of bridging between particles which may reduce the average capillary pressure of the system under consideration. Equation (13) uses the gas permeability at the full porosity and an independent parameter, $J(s)$, which is a function of saturation. It gives the best overall agreement but lacks precision. In eqn (13) the

Table 6. Comparison of capillary pressures estimated from data obtained in this work (eqn (32)) with values predicted using eqns (11)–(15b)

Powder bed	*Capillary pressure (kPa) estimated using equation number stated*					
	(32)	*(11)*	*(13)*	*(14)*	*(15a)*	*(15b)*
LA75	1·6	1·3	2·6	4·7	4·0	6·7
LA150	0·51	0·55	1·7	2·4	2·0	3·3
RA6	5·4	240	3·5	320	260	440
MA2LS	7·8	16	2·4	38	32	53

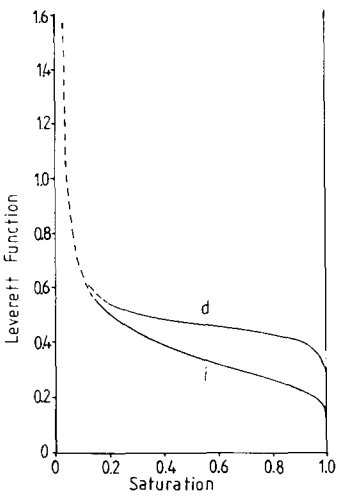

Fig. 6. The dependence of the Leverett function on saturation (from Ref. 10): d, drainage; i, imbibation.

equivalent capillary radius is represented by the square root of the permeability–porosity ratio. It accounts for the effect of saturation on the average capillary pressure of the system by reference to the curve shown in Fig. 6. The Leverett function can be expected to be more successful in correlating the drainage of the ceramic body[25] and is discussed in Part II. Equation (14) is seen to fit neither coarse nor fine powder beds. Equation (14) is obtained from the simple cubic packing model of spherical particles in the fully saturated flow regime and at much lower porosities. Such a simple geometric relation between pore size and mean particle size may thus cause errors when the equation is used for actual powder beds, particularly for a wide particle size distribution and a saturation less than one. Similar arguments apply to eqn (15), which is also based on cubic packing.

Average capillary pressure is the least accessible parameter in the flow equation (eqn (9)). Equations (11) and (13) present the best fits to the experimental data reported here when gas flow permeability is employed for K_p. Permeability and average capillary pressure are both related to pore structure. Fine pores yield high capillary pressures and low permeability, and this is reflected in the results in Tables 4a, 4b and 6. The difficulties of applying these data to sorption tests occurs where saturation is less than unity, in that large pores, which strongly influence permeability under fixed pressure difference conditions, may remain unfilled under sorption testing. A further difficulty occurs if the liquid forms a significant adsorbed layer on the solid. In the present case the thickness of adsorbed layer should approximate to the end-to-end dimensions of the wax molecule and thus be equal to 3 nm. The volume occupied by the adsorbed layer in the RA6

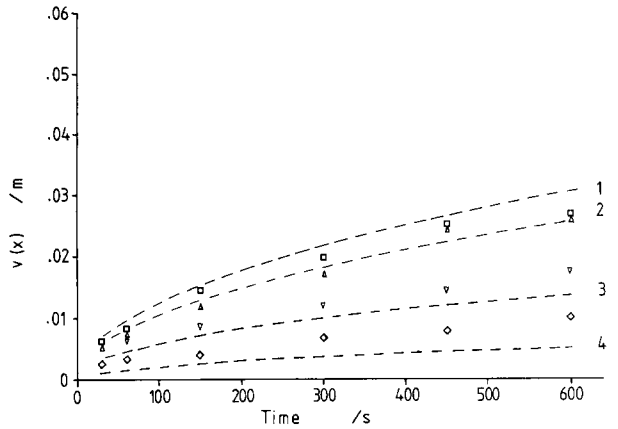

Fig. 7. Comparison of experimental flow measurements, with the curves calculated from eqn (9) using different expressions for capillary pressure: (1) □, eqn (11) for LA75; (2) △, eqn (11) for LA150; (3) ▽, eqn (13) for RA6; (4) ◇, eqn (13) for MA2LS.

powder bed was found to correspond to 2·4% of the pore volume. This is not large enough to reduce the permeability significantly.

Using the gas permeability, calculated from eqns (26)–(28) for LA75, RA6 and MA2LS, and an experimental value for LA150, the predicted sorption curve is plotted, together with the experimental points obtained from ashing results, for each powder in Fig. 7. This shows that, provided a suitable equation is used for the capillary pressure, a reasonable prediction of sorption tests can be made. However, the unfortunate fact is that no individual equation for P_c serves all powder beds.

7 Conclusions

Gas permeability has been measured for diverse ceramic powder beds as a measure of permeability to liquid flow. A range of model expressions for permeability fail to correlate with the measured values, indicating that other factors, such as agglomeration or particle bridging, influence the mass transport. Sorption curves for the flow of wax from an unlimited supply have been obtained and present a quadratic relationship with time as expected from theory, yielding a sorption constant. These show that, even with sorption from an unlimited supply, saturation is not necessarily unity for all powders. From the experimental sorption constant and the experimental permeability a value for average capillary pressure was deduced and compared with values predicted by model equations. No single expression for average capillary pressure correlates with the deduced values, but provided an appropriate equation is selected for a particular powder type the flow curve can be estimated.

Acknowledgements

The authors are grateful to Brunel University for financial support for Mrs Yuqing Bao as a visiting scholar and to Mrs K. Armstrong for typing the manuscript.

References

1. Edirisinghe, M. J. & Evans, J. R. G., Review: Fabrication of engineering ceramic by injection moulding. I: Material selection. *Int. J. High Technol. Ceram.*, **2** (1986) 1–31.
2. Edirisinghe, M. J. & Evans, J. R. G., Review: Fabrication of engineering ceramics by injection moulding. II: Techniques. *Int. J. High Technol. Ceram.*, **2** (1986) 249–78.
3. Mutsuddy, B. C., A review of binder removal processes for ceramic injection moulded parts. In *AIChE Conference on Emerging Technology in Materials*, Minneapolis, August 1987, pp. 18–20.
4. Wright, J. K. & Evans, J. R. G., Removal of organic vehicle from moulded ceramic bodies by capillary action. *Ceramics International*, **17** (1991) 79–87.
5. Curry, J. D., Apparatus and method for manufacture of articles containing controlled amount of binder. US Patent 4 001 291, filed 2 September 1975, published 8 March 1977.
6. Wiech, R. E., Manufacture of parts from particulate material. European Patent 0 032 403, filed 14 January 1981, published 22 July 1981.
7. Wei, T. & German, R. M., Injection moulded tungsten heavy alloy. *Int. J. Powder Met.*, **24** (1988) 327–35.
8. German, R. M., Theory of thermal debinding. *Int. J. Powder Met.*, **23** (1987) 237–45.
9. Beltran, V., Escardino, A., Feliu, C. & Rodrigo, Ma. D., Liquid suction by porous ceramic materials. *Brit. Ceram. Trans. J.*, **87** (1988) 64–9.
10. Leverett, M. C., Capillary behaviour in porous solids. *Trans. AIME*, **142** (1941) 152–69.
11. Carman, P. C., *Flow of Gases Through Porous Media*. Butterworths, London, 1956, p. 13.
12. Dullian, F. A. L., *Porous Media—Fluid Transport and Pore Structure*. Academic Press, London, 1979, p. 22.
13. Oyama, Y. & Yamaguchi, K., The distribution of liquid content equilibrium of powder bed in a gravitational field. *Rep. Inst. Phys. Chem. Res.*, **38** (1962) 392–400.
14. Luikov, A. V., *Heat and Mass Transfer in Capillary-porous Bodies*. Pergamon Press, Oxford, 1966, pp. 206–20.
15. Kozeny, J., About capillary conduction of water in soil (rise exhaustion and application to irrigation). Royal Academy of Science, Vienna, Proc. Class I, **136** (1927) 271–306.
16. Carman, P. C., The determination of the specific surface of powder, I. *J. Soc. Chem. Ind.*, **57** (1938) 225–34.
17. Ergun, S. & Orning, A. A., Fluid flow through randomly packed columns and fluidized beds. *Ind. Eng. Chem.*, **41** (1949) 1179–91.
18. Meyer, A. B. & Smith, D. W., Flow through porous media: Comparison of consolidated and unconsolidated materials. *Ind. Eng. Chem. Fundam.*, **24** (1985) 360–8.
19. German, R. E., Porosity and particle size effects on the gas flow characteristics of porous metals. *Powder Technol.*, **30** (1981) 81–6.
20. Lea, F. M. & Nurse, R. W., Permeability methods of fineness measurement. In *Symposium on Particle Size Analysis, (Supplement) Trans. Inst. Chem. Engrs*, **25** (1947) 47–56.
21. Scheidegger, A. E., *The Physics of Flow through Porous Media*, 3rd edn. University of Toronto Press, Canada, 1975, p. 156.

22. Scheidegger, A. E., *The Physics of Flow through Porous Media*, 3rd edn. University of Toronto Press, Canada, 1975, p. 152.
23. Bird, R. B., Stewart, W. E. & Lightfoot, E. N., *Transport Phenomena*. Wiley, New York, 1960, p. 197.
24. Watson, J. T. R., Viscosity of gases in metric units. National Engineering Laboratory, Edinburgh, 1972, p. 6.
25. Bao, Y. & Evans, J. R. G., Kinetics of capillary extraction of organic vehicle from ceramic bodies. Part II: Partitioning between porous media. *J. Eur. Ceram. Soc.*, **8** (1991) 95–105.
26. Kaelble, H. D. & Uy, K. C., A reinterpretation of organic liquid–polytetrafluorethylene surface interactions. *J. Adhesion*, **2** (1970) 50–60.